

**High-electron-temperature diagnostics of transient ionizing plasma using near-uv transitions**Ramy Doron, Ron Arad,<sup>\*</sup> Vladimir Bernshtam, and Yitzhak Maron  
*Faculty of Physics, Weizmann Institute of Science, Rehovot 76100, Israel*

Yuri Ralchenko

*Institute for Research in Electronics and Applied Physics, University of Maryland, College Park, Maryland 20742-3511, USA*

(Received 19 May 2008; published 22 September 2008)

We present spectroscopic measurements in which utilized are line-intensity ratios in the near-uv to measure electron energies of several hundred eVs, which usually necessitates the use of emission in the soft x-ray region. The main intensity ratio selected is of the B III transition  $1s^2 2s^2 S_{1/2} - 1s^2 2p^2 P_{3/2}$  (2066 Å) and the B IV transition  $1s 2s^3 S_1 - 1s 2p^3 P_2$  (2822 Å). A detailed atomic-kinetics modeling is made to demonstrate the usefulness of this atomic system for studying transient, ionizing plasmas. Here, it is applied for the characterization of high-electron energies ( $\sim 500$  eV) generated due to the rapid penetration of a magnetic field pulse into a low-collisionality plasma. Limitations of the use of the method are discussed.

DOI: [10.1103/PhysRevE.78.036410](https://doi.org/10.1103/PhysRevE.78.036410)

PACS number(s): 52.70.Kz, 32.70.Fw, 32.30.Jc

**I. INTRODUCTION**

Spectral line emission resulting from impact of electrons with energies of tens or several hundred eVs typically fall in the extreme uv or the soft x-ray bands. Spectroscopic investigations in these spectral regions are quite difficult since they necessitate the use of vacuumed grazing-incidence spectrometers. Thus, and due to the simpler absolute calibration of the visible-uv systems, it is desirable to find longer wavelength transitions ( $\lambda > 2000$  Å) that can be used for the diagnostics of hot plasmas ( $T_e > 100$  eV). This has motivated several studies aimed at finding long-wavelength transitions in highly ionized atoms that can potentially be used to monitor the properties of hot plasmas. Examples of such efforts are the studies of the forbidden transitions within complex ground configurations of highly ionized multielectron atoms [1–5]. The use of such transitions is particularly useful for pulsed-power experiments that are characterized by unfavorable access for vacuum-uv optics, and that usually offer a limited number of photons for the diagnostics.

Measurements of the electron temperature [or in a general case, the electron energy distribution (EED)] in non-LTE transient plasmas that are typical to pulsed-power experiments are highly challenging. An efficient temperature measurement is obtained by measuring a temperature-sensitive intensity ratio of spectral lines emitted from a common ion. This type of diagnostic does not depend on assumptions on the ionization distribution, and is therefore, also suitable for transient plasmas (in which the ionization balance changes rapidly and deviates significantly from its steady state value). The main difficulty in finding such line pairs arises from the additional requirement that the lines should fall in a narrow spectral region, needed for obtaining an accurate measurement of the relative line intensities. Since the temperature sensitivity of the line ratio diminishes for electron energies that exceed the energy gap between the upper levels of the two transitions, for a reliable temperature measurement this

energy gap needs to be similar to the electron temperature. Therefore, the measurement of electron temperatures of several hundred eVs is likely to require observations in short wavelengths. Indeed, temperature diagnostics in the visible uv, based on this method, are usually limited to measuring electron energies up to a few tens of eV.

In a series of previous publications [6–13] we have investigated the interaction of pulsed magnetic fields with nearly collisionless, multi-ion species plasma using various configurations of plasmas driven by current pulses. Spectroscopic methods combined with doping techniques [7,14] were employed for determining the evolution of the magnetic [6,7,10] and electric fields [13], electron density [9,10], and ion dynamics [12]. Detailed observations revealed an intriguing phenomenon in which the magnetic field only pushes the light ion-component of the plasma (protons), while, simultaneously, it rapidly penetrates into the heavier ion-component (carbon ions) [9]. This rapid magnetic field penetration is expected to be accompanied by large magnetic energy dissipation [15]. While the magnetic energy imparted to the ions was determined reliably [12], the evolution of the electron energy distribution remains a missing component in understanding the energy balance problem. Calculations performed for the specific parameters of these experiments predict that the electrons should acquire energies in excess of  $\sim 1$  keV [10]. Allegedly, measuring such electron energies using the conventional line-ratio method, mentioned above, requires observations in the soft x-ray region.

Preliminary measurements [11] using absolute intensities of visible-uv spectral lines of C III-V have indicated that the EED deviates from a Maxwellian, so that a significant portion of the electrons have energies of several hundred eVs, while the rest of the electrons remain relatively cold ( $T_e \sim 10$  eV). However, these results are subjected to large errors due to uncertainties in the C IV and C V abundances. Another problem concerning the carbon-emission measurements is the lack of spatial resolution along the line of sight (since carbon is one of the constituents of the plasma rather than a dopant in the plasma).

In an attempt to improve the measurements, line emission from a dopant He I beam, injected locally into the plasma

<sup>\*</sup>Present address: Soreq Nuclear Research Center, Yavne, Israel.

[14], was employed. Analysis of the well known  $T_e$ -sensitive He I “singlet-to-triplet” line ratio (see, for example, Refs. [16–18]), combined with absolute line intensity measurements, confirmed the deviation of the EED from a Maxwellian. The simplest scenario that is found to be consistent with the helium measurements is a relatively cold Maxwellian and an energetic electron fraction that constitutes approximately 40% of the entire electron population. However, while the He I measurements helped to establish the presence of at least two groups of electrons, they could only provide a lower limit of  $\sim 100$  eV for the energetic electrons due to the insensitivity of the He I system to higher energies. The search for a method that is based on visible-uv spectroscopy for the determination of these high electron energies is the focus of this report. A description of the entire EED measurements, including a discussion on their implications to our understanding of the rapid magnetic field penetration into the plasma, will be given in a subsequent report.

In the present paper we report on measurements of electron energies in excess of 100 eV. The measurements utilize line emission of locally injected B III and B IV. This emission is conveniently located in the near-uv region, namely, utilizing the intensity ratio of two transitions, the B III  $1s^2 2s^2 S_{1/2} - 1s^2 2p^2 P_{3/2}$  at 2066 Å and the B IV  $1s 2s^3 S_1 - 1s 2p^3 P_2$  at 2822 Å. Contrary to the conventional line-ratio method that commonly requires that both spectral lines be emitted from the same ion, here we use lines of consecutive ionization states. Nevertheless, it is shown that under the transient plasma conditions of interest, this line ratio can be a useful tool for the determination of high electron energies. Due to the large energy gap ( $\sim 200$  eV) between the upper levels of the two transitions ( $1s^2 2p^2 P_{3/2}$  for B III and  $1s 2p^3 P_2$  for B IV), the line intensity ratio maintains its temperature sensitivity up to  $\sim 500$  eV. Our analysis shows that due to the complications that arise from using lines of two ionization stages and the fact that the B IV lower level transition is metastable, this atomic system is mainly suitable for monitoring the electron temperature in transient plasmas in which the initial B IV abundance is small.

In Sec. II we provide a discussion of the main population mechanisms of the relevant levels and derive the plasma conditions under which the suggested diagnostics are applicable. In Sec. III we apply these considerations to experimentally determine the time-dependent EED in a highly transient plasma driven by a current pulse. Conclusions and a brief discussion regarding other possible applications are given in Sec. IV.

## II. ANALYSIS OF THE TEMPERATURE-SENSITIVE SYSTEM

The time-dependent collisional radiative calculations used for the atomic-kinetics analysis in the present work are described in Ref. [19]. The energy levels and radiative transition probabilities used are either taken from the NIST Atomic Spectra Database [20] or calculated using the atomic structure code by Cowan [21]. The collisional cross sections are obtained from the Coulomb-Born-exchange (CBE) code ATOM [22]. When possible, we have adopted the relevant

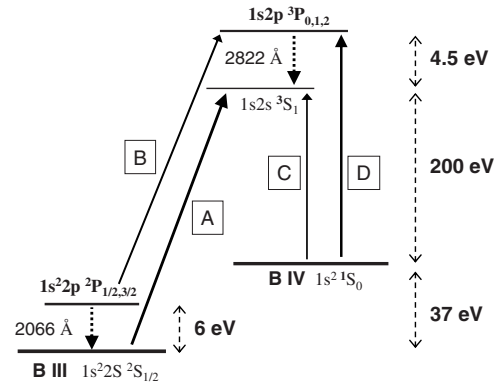


FIG. 1. The relevant energy level structure of B III and IV. The solid arrows marked by the capital letters describe the main population mechanisms responsible for the 2822-Å line intensity. The line thickness of the solid arrows gives a general idea of the relative importance of each of the population channels (assuming plasma conditions relevant to the experiment described in Sec. III).

data from the calculations and compilations appearing in Refs. [23–25]. Our model includes all the ionization stages of boron. For B III we have included the levels  $1s^2 nl$  ( $n=2-6$ ,  $l=s,p,d,f,g,h$ ) and for B IV  $1s nl$  ( $n=1-4$ ,  $l=s,p,d,f$ ), as required for the present analysis. Higher levels were assumed to be hydrogenic.

Figure 1 presents a schematic description of the relevant level structure of B III and IV. As mentioned in Sec. I, due to the energy gap of over 200 eV between the B III level ( $1s^2 2p^2 P_{3/2}$ ) and the B IV level ( $1s 2p^3 P_2$ ), the line-intensity ratio  $I_{2066 \text{ Å}}/I_{2822 \text{ Å}}$  is sensitive to rather high electron energies. We note that radiative decays from other levels of the same multiplets,  $^2P_{1/2}$  in B III and  $^3P_{0,1}$  in B IV, give rise to nearby lines (2067 Å in B III, and 2825 and 2826 Å in B IV), but these are weaker. While the line at 2066 Å arises from a resonant transition that is predominantly populated by collisional excitation from the B III ground level, the mechanisms that govern the intensity of the B IV line (2822 Å) requires further examinations.

In analyzing the intensity of the 2822-Å transition it should be noted that due to the efficient collisional excitation between the transition lower level (that is metastable),  $1s 2s^3 S_1$ , and upper-level,  $1s 2p^3 P_2$ , the population scheme of these two “triplets” is effectively reduced to a single-level populating problem. However, the slow depletion of this system, mostly through the low rate for the radiative decay of the  $1s 2p^3 P_1$  level (intercombination line) and collisional ionizations, results in a population accumulation in the triplet levels that hampers the diagnostics. Generally, since at each instance this level population reflects the history of the plasma conditions, employing the ratio  $I_{2066 \text{ Å}}/I_{2822 \text{ Å}}$  for  $T_e$ -diagnostics requires knowledge of the population initial conditions. Additionally, the very slow depletion rate makes it difficult to use this system for monitoring the cooling stage that may follow the electron heating. From a practical viewpoint, this situation limits the diagnostics to a transient ionizing plasma, in which initially, B IV abundance is small. The plasma conditions under which this picture is valid are discussed at the end of this section.

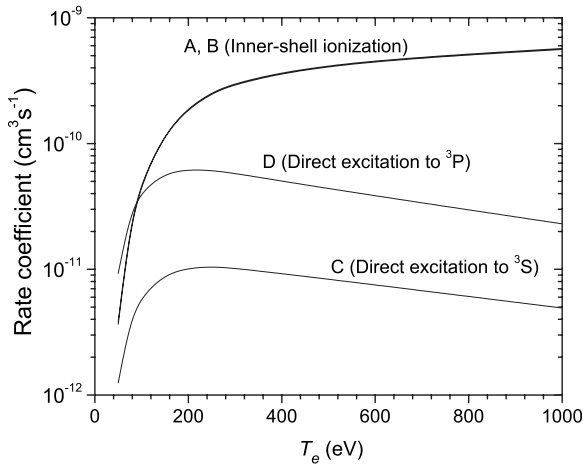


FIG. 2. The rate coefficients of the main atomic processes responsible for the B IV 2822-Å line intensity.

The main population channels responsible for the 2822-Å line emission are depicted in Fig. 1 by the solid arrows marked by the capital letters. As explained above, we limit our discussion to plasma conditions in which populating both the transition upper and lower levels contributes to the intensity of the 2822-Å line. The arrows marked by “A” and “B” represent population by inner-shell ionization from the B III ground and first excited levels, whereas arrows “C” and “D” represent collisional excitations from the B IV ground state. The calculated rate coefficients of each of the 4 channels as a function of  $T_e$  are given in Fig. 2. For studying the relative importance of each mechanism, the rate coefficients should be multiplied by the relative populations of the initial level of each transition, yielding the population flux of each channel. For ionizing plasmas, we also have to consider the temporal evolution. Initially, when there is no B IV, only inner-shell ionizations from B III are important. It can be seen from Fig. 2 that even when the B IV ground level begins to be populated, if  $T_e$  is higher than  $\sim 300$  eV, inner-shell ionizations still dominate. For example, for  $T_e = 300$  eV, if the abundance of the B IV ground state becomes 30% of the B III ground population, the population flux due to inner-shell ionizations would still exceed collisional excitations from the B IV ground state by a factor of 15.

The relative importance of the two inner-shell ionization channels (A and B) is determined by the population of the B III first excited level relative to the B III ground level. The higher the electron density is, the larger is the contribution of the inner-shell ionization from the B III excited level (channel B). The two channels become comparable for  $n_e \approx 5 \times 10^{15} \text{ cm}^{-3}$  (the B III excited-level population is insensitive to  $T_e$  for the relevant temperatures that allows for the B III ionization). The direct collisional excitation from the B IV ground state to the  $1s2p \ ^3P_2$  may begin to play a dominant role only for combinations of sufficiently high B IV abundance and  $T_e$  below 300 eV. As expected, due to the fact that the transition from the B IV ground state to the  $1s2s \ ^3S_1$  (channel C) is doubly forbidden, its contribution to the 2822-Å line intensity can be neglected.

The time window in which this diagnostic tool can be applied is limited. Obviously, this diagnostic becomes inap-

plicable when B III is completely ionized. For sufficiently high electron energies (above 200 eV), B III ionization time is only weakly dependent on the electron energy. Thus, the time window in which the diagnostic is applicable is determined by the electron density. For example, in the experiment discussed in Sec. III, the typical electron density,  $5 \times 10^{14} \text{ cm}^{-3}$ , yields a time window of  $\sim 700$  ns (although other factors, mainly related to the plasma dynamics, restrict the diagnostics to shorter times).

The discussion above leads to two important conclusions. (i) The dominance of channel A (inner-shell ionization from the B III ground state) in producing the 2822-Å line makes the accurate knowledge of the initial  $n(\text{B III})/n(\text{B IV})$  abundance ratio unimportant, as long as the B IV abundance is small. The weak dependence on the initial  $n(\text{B III})/n(\text{B IV})$  ratio is verified using collisional radiative calculations, which showed only small differences ( $\sim 10\%$ ) in the line ratio  $I_{2066 \text{ Å}}/I_{2822 \text{ Å}}$  for different initial B IV relative abundance (in the 5–15 % range). This behavior is useful for the application described in Sec. III, where it is known that initially the B IV is a minority, while its accurate abundance could not be determined. (ii) Since in an ionizing plasma both the inner-shell ionization via the metastable (channel A) and the collisional excitation from the B IV ground state (channel D) are in fact a two-step process (ionization from B III followed by collisional excitations to  $1s2p \ ^3P_{0,1,2}$ ), their rates depend on  $n_e^2$ . Therefore, the large contributions of channels B and D to the 2822-Å line intensity, combined with the linear  $n_e$  dependence of the 2066-Å line intensity, makes the ratio  $I_{2066 \text{ Å}}/I_{2822 \text{ Å}}$  also  $n_e$  sensitive, which is not desirable for temperature diagnostics.

Fortunately, the temporal evolution of the 2066-Å line intensity offers an independent means to simultaneously determine the electron density. Since this is a resonant line, its intensity closely follows the B III abundance, that is very sensitive to the electron density, while at the same time, for the temperature range of interest ( $T_e > 100$  eV), it is only weakly dependent on the temperature. This behavior is demonstrated in Fig. 3, in which the upper part presents the calculated evolution of the 2066-Å line intensity for three different electron densities in the range from  $3 \times 10^{13}$  to  $2 \times 10^{14} \text{ cm}^{-3}$  for  $T_e = 300$  eV. For  $n_e = 10^{14} \text{ cm}^{-3}$  we also plotted the intensity evolution at temperatures of 200 and 400 eV to show the weak  $T_e$  dependence. In the lower part of the figure we give the evolution of the abundance ratio  $n(\text{B IV})/n(\text{B III})$ . In all calculations we assume the initial condition is 100% B I, and assume a constant density and temperature. Such a scenario may correspond to a case where a boron minority is introduced into the plasma, so that the plasma parameters are not significantly perturbed by the injected boron. At early times the intensity of the 2066-Å line rises due to the ionization of B II into B III. Later, when the ionization of B III into B IV dominates (see the lower part of Fig. 3), the intensity drops. The peak intensity in each curve is obtained for times that correspond to the B III peak abundance. It can be seen from the figure that varying the electron density by a factor of 2 results in a totally different behavior of the line intensity evolution, while a variation of the electron temperature (for the same density) has a small effect.

The nature of the  $n_e$  sensitivity of the ratio  $I_{2066 \text{ Å}}/I_{2822 \text{ Å}}$  is rather complex, since this sensitivity is both  $n_e$  and time

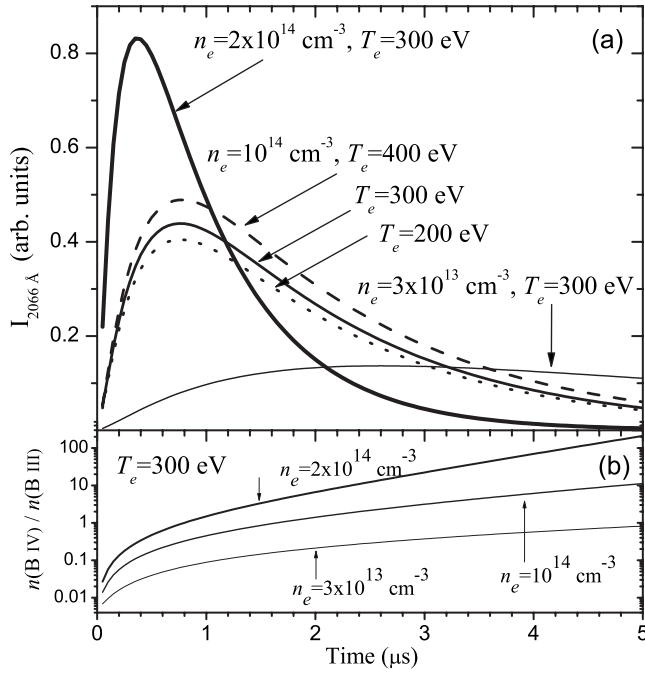


FIG. 3. (a) The intensity of the B III 2066-Å line as a function of time calculated for three electron densities  $n_e = 3 \times 10^{13}$ ,  $10^{14}$ , and  $2 \times 10^{14} \text{ cm}^{-3}$ , for  $T_e = 300 \text{ eV}$ . For  $n_e = 10^{14} \text{ cm}^{-3}$  the intensity is also calculated for  $T_e = 200$  and  $400 \text{ eV}$ . (b) The corresponding evolution of the abundance ratio  $n(\text{B IV})/n(\text{B III})$ .

dependent. In a steady state, the upper level population of the 2822-Å line  $n_{3P}$  is given by

$$n_{3P} = \frac{n_e(n_{1S}Q_{1S \rightarrow 3P} + n_{3S}Q_{3S \rightarrow 3P} + n_{2P}S_{2P \rightarrow 3P})}{A_{3P \rightarrow 3S} + n_e(Q_{3P \rightarrow 3S} + S_{3P \rightarrow B V})}, \quad (1)$$

where  $^3P$ ,  $^1S$ ,  $^3S$ , and  $^2P$  represent, respectively, the B IV levels  $1s2p\ ^3P_2$ ,  $1s^2\ ^1S_0$ , and  $1s2s\ ^3S_1$  and the B III level  $1s^22p\ ^2P_{1/2}$ . The symbols  $Q$ ,  $S$ , and  $A$  are, respectively, the collisional-(de)excitation and -ionization rate coefficients, and the radiative decay rate. In Eq. (1), the numerator describes the processes that populate the upper level of the 2822-Å line, whereas the denominator describes the level depopulation through the radiative decay, collisional deexcitation to the metastable level, and collisional ionization into B V (the ionization term to B V, includes also excitations from  $^3P$  to higher levels of B IV followed by ionization). Even though Eq. (1) describes a steady-state solution it provides an insight into the role of  $n_e$ . Assuming that initially, the populations of the three levels appearing in the numerator are all linearly dependent on  $n_e$ , the numerator is proportional to  $n_e^2$ . Therefore, the  $n_e$  dependence of the  $^3P$  level population, and hence also that of the 2822-Å line intensity, are determined by the ratio between the two terms appearing in the denominator, namely, the  $n_e$ -dependent collisional depopulation rate and the  $n_e$ -independent depopulation rate due to the radiative decay. For low electron densities, where the collisional depopulation rate is negligible compared to the radiative decay rate, the 2822-Å-line intensity is proportional to  $n_e^2$ ; while for high densities, where the collisional depopulation is more impor-

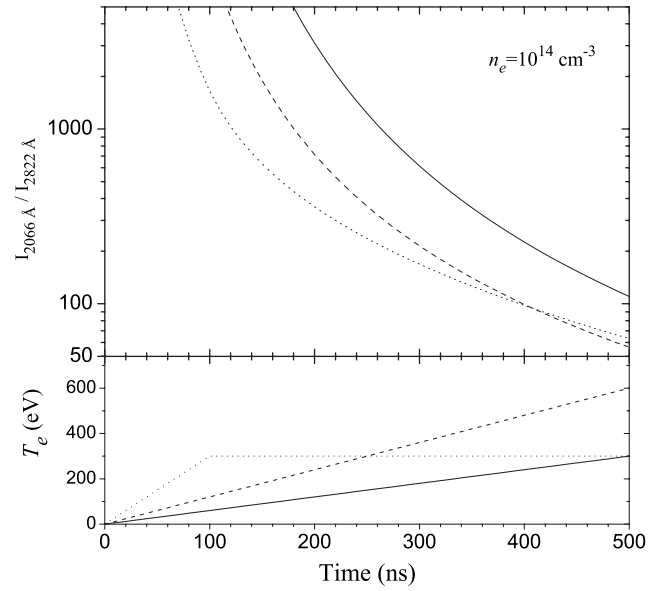


FIG. 4. (a) The calculated line-intensity ratio  $I_{2066\text{Å}}/I_{2822\text{Å}}$  as a function of time. The three curves correspond to three plasma models shown in (b):  $T_e$  rises from 0 to 300 eV within 500 ns (solid),  $T_e$  rises from 0 to 600 eV within 500 ns (dashed), and  $T_e$  rises from 0 to 300 eV within 100 ns and then remains constant (dotted). All models assume  $n_e = 10^{14} \text{ cm}^{-3}$  and neutral boron atoms at  $t=0$ .

tant, the line intensity has a weaker  $n_e$  dependence. Since at these early times the 2066-Å resonant line depends linearly on  $n_e$ , the sensitivity of the ratio  $I_{2066\text{Å}}/I_{2822\text{Å}}$  to uncertainties in  $n_e$  is proportional to the  $n_e$  uncertainty for low electron densities, while the ratio becomes nearly  $n_e$  independent for high densities.

However, at later times, the ionization of B III into B IV begins to play a crucial role. At these times the ionization of B III is not compensated for by ionization from B II into B III, hence the intensity of the B III 2066-Å line decreases with increasing  $n_e$  (due to the faster collisional ionization), while the intensity of the B IV 2822-Å line increases with increasing  $n_e$ . The result is an increased  $n_e$  sensitivity of the ratio  $I_{2066\text{Å}}/I_{2822\text{Å}}$ . To conclude, our analysis shows that the  $n_e$  dependence of the ratio  $I_{2066\text{Å}}/I_{2822\text{Å}}$  becomes important mainly when the ionization balance shifts towards B IV. Thus, as further discussed in Sec. III, in the present experiment, where the B III is moderately ionized, the inferred electron energies are weakly sensitive to uncertainties in  $n_e$ .

We emphasize that unlike the common temperature diagnostic method, where ideally it is possible to uniquely assign a temperature to each line ratio, here, due to the complexity arising from the use of a two-ionization-stage system, inferring the electron temperature requires the application of a detailed, time-dependent modeling that uses the initial level population and the known electron density evolution as inputs. To demonstrate the use of the ratio  $I_{2066\text{Å}}/I_{2822\text{Å}}$  as a means for the diagnostics, we present in Fig. 4 the calculated temporal evolution of the ratio for three simple cases of transient plasmas. As shown in the lower part of Fig. 4, simulated are plasmas with  $T_e$  rising linearly from 0 to 300 eV within 500 ns,  $T_e$  that rises to 600 eV within 500 ns, and  $T_e$  that rises to 300 eV within 100 ns and then remains constant.

The calculations assume a constant  $n_e = 10^{14} \text{ cm}^{-3}$  and neutral boron atoms at  $t=0$ . At early times (close to the electron heating onset), when the 2822-Å line is very weak, as reflected by the high ratios, no reliable data can be obtained. Therefore, additional, more accurate information on the time of the heating onset is required for improving the simulation of the experimental ratio. This could be done, for example, using the relative intensities of lines arising from B III high-lying levels (e.g., the  $3d-4f$  at 2077 Å or the  $n=4 \rightarrow n=5$  transitions around 4500 Å). As can be seen in Fig. 4, the differences between the different models are most pronounced at early times. Hence, the experimental challenge is to accurately measure the 2822-Å line intensity as early as possible.

It is interesting to note that for very low electron densities the diagnostics open the possibility to also monitor cooling conditions. For such densities, contrary to the situation discussed in the above (where the electron-transfer rate between the two triplet levels is assumed to be higher than all other populating or depopulating mechanisms of these levels), the collisional excitation rate from the metastable level  $1s2s^3S^1$  is lower than the radiative decay rate of this level. For  $n_e < 10^7 \text{ cm}^{-3}$  the population accumulation in the triplet levels ceases, and thus electron cooling can be studied.

For densities higher than the range addressed in the present work, the analysis is similar to that discussed above; however, it is rather more involved since more levels need to be taken into account. In particular, for  $n_e > 10^{17} \text{ cm}^{-3}$  the atomic model must include B V since the level  $1s2p^3P_2$  is depleted faster through ionization into B V than through the radiative decay that produces the 2822-Å line.

Finally, in applying the method, since the 2066-Å B III line arises from a resonant transition, opacity effects should be considered. However, these are negligible in the experiment here addressed.

### III. APPLICATION TO A PLASMA DRIVEN BY A CURRENT PULSE

The diagnostic method here suggested is applied to study the formation of the energetic electrons during the propagation of a pulsed magnetic field through a plasma. The experiments are performed using a pulsed current driven through a plasma bridge between two electrodes, in a configuration similar to that used for plasma opening switches (see, for example, Ref. [26]). The experimental setup is described in detail in previous papers [10,12]. In brief, it consists of two planar 14-cm wide electrodes separated by a 2.5-cm gap. An 8-cm long (in the propagation direction of the magnetic field) region is prefilled with plasma using a surface-flashover (flashboard) plasma source that is mounted outside the gap. The plasma is composed of protons and carbon ions and its initial parameters (prior to the current application) are  $n_e \sim 5 \times 10^{14} \text{ cm}^{-3}$  and  $T_e \sim 6 \text{ eV}$  [27]. A pulsed current rising to 150 kA in 400 ns that produces a magnetic field with a peak amplitude of 1 T is applied and propagates rapidly through the plasma in a form of a  $\sim 1$ -cm wide current channel [10]. For the visible-uv spectroscopic observations, the outputs of two 1-m spectrometers are attached to a gated

(5 ns), intensified, charge-coupled device camera and to an array of photomultiplier tubes that provide 7 ns temporal resolution. The optical system is absolutely calibrated, allowing for the determination of the upper level population of the measured transitions. Plasma doping techniques are employed to obtain spatially resolved spectroscopic measurements. Two doping methods are used: a surface flashover method for producing dopants of solid material [12] and a gas-doping technique [14].

As described in Sec. I, time-dependent measurements of transitions of He I dopant yielded rather clear indications of a significant deviation of the EED from a Maxwellian. These measurements showed that  $(40 \pm 10)\%$  of the electrons acquire an energy in excess of 100 eV. We thus use the B III and B IV line emissions to determine the energy of these energetic electrons.

A beam of boron ions is injected into the middle of the prefilled plasma. The parameters of the surface flashover that produce the boron dopant are selected to yield a 2-cm-wide boron column, with similar B II and B III ionic densities of  $\sim 1.5 \times 10^{12} \text{ cm}^{-3}$  (determined spectroscopically using the absolute intensities of the B II line at 3451 Å, the B III line at 2066 Å, and the known  $n_e$  and  $T_e$  of the prefilled plasma). Under these conditions the opacity effects of the 2066-Å transition of interest can be neglected. Comparison between spectra obtained in experiments with B dopants to those obtained without B injection allows for an unambiguous identification of the relatively low-intensity B IV 2822-Å line even under conditions in which its intensity is just above the noise level.

Studying spectroscopically the B IV initial abundance is difficult. In principle, due to the large difference between the energy threshold required to ionize B III (37 eV) and that required to populate the B IV first excited level ( $\sim 200 \text{ eV}$ ), B IV can be present at the ground state at significant abundances, although undetectable. However, in our experiment the initial B IV abundance can at most reach a few percent (the B II and B III about equally constitute most of the boron plasma), as verified by the collisional radiative models of the boron ionization distribution, assuming the present  $n_e$  of  $\sim 5 \times 10^{14} \text{ cm}^{-3}$  and  $T_e$  up to 10 eV. As explained in Sec. II, such initial conditions are most suitable for applying the present diagnostics for the rapid heating that ensues when the pulsed current is applied.

We note that in the collisional radiative models we have neglected ion-impact collisional excitations and ionizations (and inverse processes). This is justified by the relatively low ion energies [12], for which the estimated ion-impact collisional excitation and ionization rate coefficients for the relevant transitions are much smaller than the corresponding electron-impact rate coefficients. In addition, charge-exchange processes are also neglected, mainly due to the very low neutral density (a few percent relative to  $n_e$ ) at the observed volume in the middle of the interelectrode gap. The situation might be somewhat different very close to the electrodes, where neutrals are more abundant due to electrode sputtering. Indeed, measurements very close (1 mm) to the electrodes have yielded moderate enhancement of some line emissions, which we attribute in part to charge-exchange processes with hydrogen. However, due to the short time

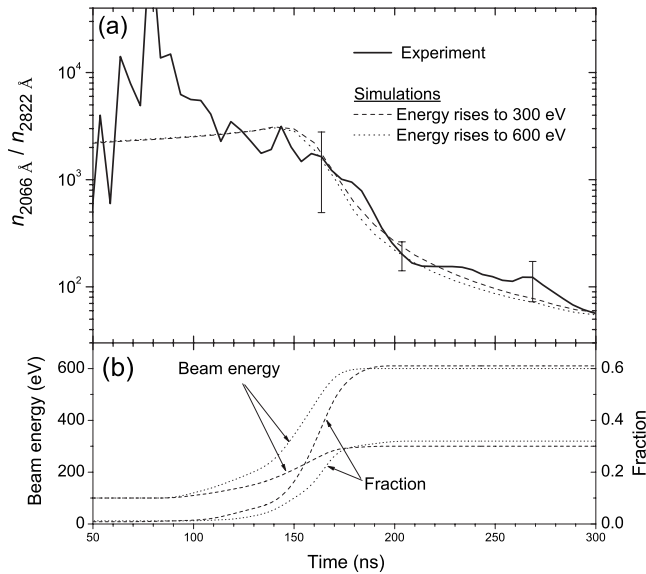


FIG. 5. (a) The time-dependent upper level population ratio  $n_{2066 \text{ \AA}} / n_{2822 \text{ \AA}}$ . The solid, bold curve represents the experimental result (as determined from the measured line intensities), while the thin dashed and dotted curves represent two simulation results. (b) The parameters (the energetic electron fraction and energy) used for the simulations shown in (a). Time=0 represents the application of the current pulse.

scales of the experiment and taking into account the measured ion velocities, post charge-exchange ions (or atoms) do not have sufficient time to flow from near the electrode into the volume here observed (10 mm from the electrode).

In Fig. 5 we present the measured time-dependent upper level population ratio  $n_{2066 \text{ \AA}} / n_{2822 \text{ \AA}}$ , together with the results of collisional-radiative calculations. The errors shown also represent the shot-to-shot irreproducibility. The high (noisy) ratio seen at early times is due to the low intensity of the B IV 2822-Å line. After about 120 ns, the propagating current-channel (and the magnetic field front it produces) arrives at the point of observation and the resultant electron heating causes the ratio to drop. This result is modeled using time-dependent collisional radiative calculations for a variety of EEDs consisting of two distinct electron populations: a relatively cold Maxwellian and a component of energetic electrons.

The time-dependent electron density required for these simulations is inferred from the intensity evolution of the B III 2066-Å line [10]. The temperature of the Maxwellian population, which affects the results only weakly, was assumed to rise from an initial temperature of 6 eV to  $15 \pm 5$  eV, based on the C III- and He I-emission measurements to be presented in a subsequent report. The fraction and energy of the energetic electrons serve as free parameters for the calculations. In each time step of the calculations these two parameters are varied to produce a good fit to the experimental ratio. Since there are two free parameters we obtain a set of solutions, namely, each ratio value can be reproduced by different combinations of energy and fraction that span the set of solutions. We find that the solutions that provide a reasonably good agreement to the experi-

ment yield a similar average electron energy, that rises from  $6.5 \pm 1$  eV at  $\sim 120$  ns up to  $200 \pm 50$  eV at  $\sim 200$  ns. An example of such two solutions is given in Fig. 5 by the dashed and dotted curves, which, respectively, represent a model that assumes an energetic electron fraction that rises to 61% with an energy of 300 eV, and a model that assumes a fraction that rises to 32% with an energy of 600 eV [see Fig. 5(b)]. We emphasize that the set of solutions we choose, represented in Fig. 5, is not unique; it is obtained assuming the energetic electron fraction and energy are smooth, monotonic functions of time.

At late times ( $>200$  ns), our models, which assume the electron energy remains high [see Fig. 5(b)], give values close to the lower limit of the experimental error bars [e.g., at 270 ns in Fig. 5(a)]. This behavior suggests that contrary to our models, the electron energy somewhat drops at late times. However, as explained in Sec. II, due to the population accumulation of the B IV metastable level, it is difficult to diagnose a cooling stage. In addition, the different dynamics of B III and B IV under the influence of the magnetic field, due to their different charge-to-mass ratios [12], may remove some of the B IV from the line-of-sight faster than B III, leading to somewhat larger experimental line-ratios at late times.

The existence of a set of solutions with a common approximate average electron energy results from the independence of the 2066-Å line intensity on the details of the EED and the dominance of a single populating mechanism for the upper level of the 2822-Å line (mechanism B in Fig. 1), where the latter becomes monotonically more effective with increasing electron energy (in the relevant energy range). Thus, reducing the electron energy in the model can be compensated for by an increased energetic electron fraction, yielding similar line intensity ratios. However, since for  $T_e > 350$  eV the increase of the rate coefficient for populating the 2822-Å-line upper level becomes more moderate, lower fractions are associated with somewhat higher mean electron energies. For example, assuming an energetic electron fraction of up to 60% requires an energy of 300 eV, yielding an average electron energy of 185 eV, while assuming a fraction of only 20% requires an energy of 1200 eV, yielding an average energy of 230 eV. A solution that assumes an energetic electron fraction of  $(40 \pm 10)\%$  at  $t=200$  ns, and that is consistent with the He I measurements, narrows down the possible energy of the energetic electrons to  $500 \pm 130$  eV.

The uncertainty of 130 eV in the electron energy is a result of the combined uncertainties in the values of the energetic-electron fraction (inferred from the He measurements) and in the experimental ratio, and assuming the atomic data are known to within an accuracy of 10%. We also examined the sensitivity of the result to uncertainties in the electron density used for the simulations. Since the electron heating occurs on a time scale that is shorter than the B III ionization time (as is verified by collisional radiative models showing that the B IV abundance increases up to a maximum of 25%), then based on the discussion given in Sec. II, for this moderate ionization-balance shift, the ratio  $I_{2066 \text{ \AA}} / I_{2822 \text{ \AA}}$  is rather weakly sensitive to uncertainties in  $n_e$ . Indeed, assuming a reasonable uncertainty of 20% in  $n_e$ , and keeping all the other parameters of the simulations constant, we obtain ratios that are different by less than 15%.

This additional uncertainty brings the energy value of the energetic electrons to  $500 \pm 160$  eV and the mean electron energy to  $210 \pm 70$  eV.

#### IV. CONCLUSIONS

A method is developed for measuring electron energies of several hundred eVs in transient ionizing plasma using spectroscopic observations in the near-uv region, thereby avoiding the need to employ vacuum-uv or soft x-ray diagnostics. Unlike the conventional  $T_e$ -diagnostic method that is based on line intensity ratios in a single ionic charge state, we here employ an intensity ratio of spectral lines emitted from B III and B IV. The applicability of the technique is limited to transient ionizing plasmas, due to the use of consecutive ionization stages and the fact that the lower-level of the B IV transition is metastable.

In the present work the method is applied for a plasma with an electron energy distribution known to consist of a relatively cold Maxwellian component and a fraction of  $\sim 40\%$  of energetic electrons with an energy higher than

100 eV. The line-intensity ratio ( $I_{2066 \text{ \AA}}/I_{2822 \text{ \AA}}$ ) here employed allows for determining the energy of the energetic electrons to be  $500 \pm 160$  eV. This technique could also be applied for sub-keV temperature measurements in tokamaks, where the typical densities of  $\sim 10^{13}$ – $10^{14}$  cm $^{-3}$  yield a diagnostic time window of  $\sim 4$ – $40$   $\mu$ s, determined by the ionization time of B III.

One may suggest expanding this method, employing near-uv line emissions, to neighboring elements. However, for higher- $Z$  elements, measuring the corresponding transitions requires vacuum arrangements, while using ions of lower  $Z$  elements (and therefore lower charge states) is limited to diagnostics of lower electron energies, where the conventional, simpler, single-ion method can be applied using visible-uv emission.

#### ACKNOWLEDGMENTS

This work was supported in part by the Israel Science Foundation (ISF) and by Sandia National Laboratories (USA).

- 
- [1] G. A. Doschek and U. Feldman, *J. Appl. Phys.* **47**, 3083 (1976).
- [2] S. Suckewer, *Phys. Scr.* **23**, 71 (1981).
- [3] E. Hinnov, S. Suckewer, S. Cohen, and K. Sato, *Phys. Rev. A* **25**, 2293 (1982).
- [4] U. Feldman, P. Indelicato, and J. Sugar, *J. Opt. Soc. Am. B* **8**, 3 (1991).
- [5] R. Doron and U. Feldman, *Phys. Scr.* **64**, 319 (2001).
- [6] M. Sarfaty, Y. Maron, Ya. E. Krasik, A. Weingarten, R. Arad, R. Shpitalnik, and A. Fruchtman, *Phys. Plasmas* **2**, 2583 (1995).
- [7] R. Shpitalnik, A. Weingarten, K. Gomberoff, Ya. Krasik, and Y. Maron, *Phys. Plasmas* **5**, 792 (1998).
- [8] Ya. E. Krasik and A. Weingarten, *IEEE Trans. Plasma Sci.* **26**, 208 (1998).
- [9] A. Weingarten, R. Arad, Y. Maron, and A. Fruchtman, *Phys. Rev. Lett.* **87**, 115004 (2001).
- [10] R. Arad, K. Tsigtukin, A. Fruchtman, J. D. Huba, and Y. Maron, *Phys. Plasmas* **10**, 112 (2003).
- [11] R. Doron, R. Arad, K. Tsigtukin, D. Osin, A. Weingarten, A. Starobinets, V. A. Bernshtam, E. Stambulchik, Yu. V. Ralchenko, Y. Maron, A. Fruchtman, A. Fisher, J. D. Huba, and M. Roth, *Phys. Plasmas* **11**, 2411 (2004).
- [12] R. Arad, K. Tsigtukin, Y. Maron, and A. Fruchtman, *Phys. Plasmas* **11**, 4515 (2004).
- [13] K. Tsigtukin, R. Doron, E. Stambulchik, V. Bernshtam, Y. Maron, A. Fruchtman, and R. J. Comisso, *Phys. Rev. E* **76**, 046401 (2007).
- [14] R. Arad, L. Ding, and Y. Maron, *Rev. Sci. Instrum.* **69**, 1529 (1998).
- [15] A. Fruchtman, *Phys. Rev. A* **45**, 3938 (1992).
- [16] S. P. Cunningham, *Conference on Thermonuclear Reactions*, University of California, Laboratory of Radiation, Livermore (U.S. Atomic Energy Commission, Washington, DC, 1955), p. 289.
- [17] R. J. Sovie, *Phys. Fluids* **7**, 613 (1964).
- [18] N. Brenning, *J. Quant. Spectrosc. Radiat. Transf.* **24**, 293 (1980).
- [19] Yu. V. Ralchenko and Y. Maron, *J. Quant. Spectrosc. Radiat. Transf.* **71**, 609 (2001).
- [20] Yu. V. Ralchenko, A. E. Kramida, J. Reader, and NIST ASD Team, <http://physics.nist.gov/PhysRefData/ASD/index.html#Team>, NIST Atomic Spectra Database (version 3.1.3), available at <http://physics.nist.gov/asd3> [2008 January 1], National Institute of Standards and Technology, Gaithersburg, MD.
- [21] R. D. Cowan, *The Theory of Atomic Structure and Spectra* (University of California Press, Berkeley, 1981).
- [22] I. I. Sobelman, L. A. Vainshtein, and E. Y. Yukov, *Excitation of Atoms and Broadening of Spectral Lines* (Springer-Verlag, Heidelberg, 1995).
- [23] V. I. Fisher, Yu. V. Ralchenko, V. A. Bernshtam, A. Goldgirsh, Y. Maron, L. A. Vainshtein, and I. Bray, *Phys. Rev. A* **56**, 3726 (1997).
- [24] V. A. Bernshtam, Yu. V. Ralchenko, and Y. Maron, *J. Phys. B* **33**, 5025 (2000).
- [25] A. Starobinets, I. Bray, L. A. Vainshtein, Yu. Ralchenko, and Y. Maron, *Phys. Scr.* **67**, 500 (2003).
- [26] C. W. Mendel, Jr. and S. A. Goldstein, *J. Appl. Phys.* **48**, 1004 (1977); *IEEE Trans. Plasma Sci.* **PS-15** (6), (1987), special issue on plasma opening switches.
- [27] R. Arad, K. Tsigtukin, Yu. V. Ralchenko, and Y. Maron, *Phys. Plasmas* **7**, 3797 (2000).